

This document is confidential and is proprietary to the American Chemical Society and its authors. Do not copy or disclose without written permission. If you have received this item in error, notify the sender and delete all copies.

## Fe-N-doped Carbon Capsules with Outstanding Electrochemical Performance and Stability for the Oxygen Reduction Reaction in Both Acid and Alkaline Conditions

Journal:	<i>ACS Nano</i>
Manuscript ID	nn-2016-01247p.R2
Manuscript Type:	Article
Date Submitted by the Author:	12-May-2016
Complete List of Authors:	Ferrero, Guillermo A.; Instituto Nacional del Carbon (CSIC), Preuss, Kathrin; Queen Mary University of London, Marinovic, Adam; Queen Mary University of London, School of Engineering and Materials Science Jorge, Ana; University College London, Chemistry Department; Queen Mary University of London, Materials Research Institute, School of Engineering and Materials Mansor, Noramalina; UCL, Chemical Engineering Brett, Dan; UCL, Chemical Engineering Fuertes, Antonio; Research center, Chemistry of Materials Sevilla Solis, Marta; Instituto Nacional del Carbón, Química de Materiales Titirici, Maria-Magdalena; Queen Mary University of London, School of Engineering and Materials Science

SCHOLARONE™  
Manuscripts

1  
2  
3 **Fe-N-doped Carbon Capsules with Outstanding**  
4  
5 **Electrochemical Performance and Stability for the Oxygen**  
6  
7 **Reduction Reaction in Both Acid and Alkaline Conditions**  
8  
9

10  
11  
12  
13 Guillermo A. Ferrero,<sup>a</sup> Kathrin Preuss,<sup>b</sup> Adam Marinovic,<sup>b</sup> A. Belen Jorge,<sup>c,d</sup>  
14 Noramalina Mansor,<sup>e</sup> Dan J. L. Brett,<sup>e</sup> Antonio B. Fuertes,<sup>a</sup> Marta Sevilla,<sup>a,\*</sup>  
15 Maria-Magdalena Titirici<sup>b,\*</sup>  
16  
17  
18  
19

20 <sup>a</sup> Instituto Nacional del Carbón (CSIC), P.O. Box 73, Oviedo 33080, Spain

21 <sup>b</sup> School of Engineering and Materials Science, Queen Mary University of  
22 London, Mile End Road, E1 4NS, London, UK  
23  
24

25 <sup>c</sup> Department of Chemistry, University College London, WC1H 0AJ, London, UK  
26

27 <sup>d</sup> Materials Research Institute, School of Engineering and Materials, Queen  
28 Mary University of London, E1 4NS, London, UK  
29

30 <sup>e</sup> Department of Chemical Engineering, University College London, London  
31 WC1E 7JE, UK  
32

33  
34  
35 \* Corresponding authors: martasev@incar.csic.es (M. Sevilla),

36 m.m.titirici@qmul.ac.uk (M.-M. Titirici)  
37  
38  
39  
40  
41  
42  
43

44 **Abstract**

45  
46 High surface area N-doped mesoporous carbon capsules with iron traces  
47 exhibit outstanding electrocatalytic activity for the oxygen reduction reaction  
48 (ORR) in both alkaline and acidic media. In alkaline conditions, they exhibit a  
49 more positive onset (0.94 V vs. RHE) and half-wave potentials (0.83 V vs. RHE)  
50 than commercial Pt/C, while in acidic media the onset potential is comparable to  
51 that of commercial Pt/C with a peroxide yield lower than 10 %. The Fe-N-doped  
52  
53  
54  
55  
56  
57  
58  
59  
60

1  
2  
3 carbon catalyst combines the high catalytic activity with remarkable  
4  
5 performance stability (3500 cycles between 0.6 and 1.0 V vs. RHE), which  
6  
7 stems from the fact that iron is coordinated to nitrogen. Additionally, the newly  
8  
9 developed electrocatalyst is unaffected by the methanol cross-over effect in  
10  
11 both acid and basic media, contrary to commercial Pt/C. The excellent catalytic  
12  
13 behavior of the Fe-N-doped carbon, even in the more relevant acid medium, is  
14  
15 attributable to the combination of chemical functions (N-pyridinic, N-quaternary  
16  
17 and Fe-N coordination sites) and structural properties (large surface area, open  
18  
19 mesoporous structure and short diffusion paths), which guarantees a large  
20  
21 number of highly active and fully accessible catalytic sites and rapid mass-  
22  
23 transfer kinetics. Thereby, this catalyst represents an important step forward  
24  
25 towards replacing Pt catalysts with cheaper alternatives. In this regard, an  
26  
27 alkaline anion exchange membrane fuel cell was assembled with the Fe-N-  
28  
29 doped mesoporous carbon capsules as the cathode catalyst providing current  
30  
31 and power densities matching those of a commercial Pt/C, which glimpses the  
32  
33 practical applicability of the Fe-N-carbon catalyst.  
34  
35  
36  
37  
38  
39  
40  
41  
42

43 **Keywords:** carbon nanomaterial, nitrogen-doping, oxygen reduction reaction,  
44  
45 non-noble metal catalysts, capsule  
46  
47  
48  
49  
50  
51  
52  
53  
54  
55  
56  
57  
58  
59  
60

1  
2  
3 One major limitation in the performance of proton exchange membrane  
4 (PEM) fuel cells is the sluggish kinetics of the oxygen reduction reaction (ORR)  
5 occurring at the cathode.<sup>1, 2</sup> This issue compromises their widespread utilization  
6 and commercialization. Traditionally, platinum has been considered as the best  
7 catalyst for the ORR, taking into account its high activity *via* four electrons  
8 transfer leading to water as the final product. However, platinum is scarce, its  
9 performance degrades in time and it is very expensive.<sup>3, 4</sup> Considerable  
10 research efforts have been directed towards the discovery of cost-effective  
11 materials exhibiting comparable catalytic performance to platinum, while  
12 showing a better tolerance towards CO poisoning. The development of non-  
13 precious metal catalysts<sup>5-8</sup> and metal-free catalysts<sup>9</sup> has gained increasing  
14 research attention due to their good catalytic activity towards ORR, low cost and  
15 good durability. Despite exhaustive research in non-precious metal and metal-  
16 free ORR catalysts, the challenge remains to be able to maintain or even  
17 increase the electrochemical performance and durability at the PEMFC's  
18 cathode.<sup>10, 11</sup>

19  
20  
21  
22  
23  
24  
25  
26  
27  
28  
29  
30  
31  
32  
33  
34  
35  
36  
37  
38 Heteroatom-doped carbon materials are promising alternatives as ORR  
39 catalysts -often *via* a 4e<sup>-</sup> route similar to platinum-, with high current densities  
40 and high onset potential.<sup>12</sup> Among various dopants, nitrogen has been  
41 extensively studied due to its enhanced electrocatalytic activity for ORR, in  
42 addition to other beneficial properties, such as increased electrical conductivity  
43 and oxidation stability.<sup>13-16</sup> The main drawback of N-doped metal-free carbon  
44 materials when used as electrocatalysts is their poor performance and poor  
45 stability in acidic media.<sup>2, 17-20</sup> Indeed, most reports show excellent N-doped  
46 electrocatalysts in alkaline media,<sup>21-25</sup> but only very few groups have shown a

1  
2  
3 good performance in acid media.<sup>26-29</sup> Furthermore, even if previously reported  
4  
5 N-doped metal-free carbons exhibited a good performance in acid media, their  
6  
7 performance drastically decreased after several cycles due to the degradation  
8  
9 of the carbon matrix.<sup>2, 12, 24</sup> To overcome these difficulties, N-doping has been  
10  
11 combined with the addition of non-precious metals such as cobalt or iron,  
12  
13 leading to catalysts that exhibit a higher activity, long-term stability and better  
14  
15 tolerance to poisons than only N-doped carbons.<sup>27, 30, 31</sup> Within this context, one  
16  
17 of the most promising catalysts is a carbon material containing Fe–N moieties  
18  
19 on the surface (Fe–N–C) which, even with only iron traces, shows a higher  
20  
21 catalytic activity.<sup>11, 32-34</sup> The main active site is believed to be iron coordinated to  
22  
23 nitrogen, which has been demonstrated to play a major role in the ORR  
24  
25 process.<sup>11, 35</sup>  
26  
27  
28  
29

30  
31 Herein, we report on N-doped mesoporous carbon capsules with iron traces  
32  
33 as ORR electrocatalyst with remarkable performance and stability under both  
34  
35 acid and alkaline conditions. This material was synthesized by using pyrrole as  
36  
37 carbon precursor and non-porous core/mesoporous shell silica particles as  
38  
39 sacrificial template. The use of FeCl<sub>3</sub> for the oxidative polymerization of pyrrole  
40  
41 leads to a N-doped carbon material with traces of iron, which cannot be  
42  
43 dissolved even after harsh acid treatment as a consequence of the fact that part  
44  
45 of it is coordinated to nitrogen and the other is as Fe<sub>3</sub>C encapsulated in a  
46  
47 relatively thick graphitic layer (~ 15 nm). Although the use of pyrrole as carbon  
48  
49 precursor for ORR catalysts has already been reported,<sup>36-38</sup> the electrocatalytic  
50  
51 activity of such catalysts in acid electrolyte is far from that of commercial  
52  
53 platinum. However, our ORR electrocatalysts exhibit several properties that are  
54  
55 highly important for an effective performance: a) a large number of nitrogen  
56  
57  
58  
59  
60

1  
2  
3 functional groups within the carbon framework due to the use of pyrrole as the  
4 carbon precursor; b) the presence of nitrogen-iron coordination sites; c) a high  
5 specific surface area ( $\sim 1600 \text{ m}^2 \text{ g}^{-1}$ ) and a porosity made up of uniform  
6 mesopores ( $\sim 3.8 \text{ nm}$ ) due to the mesoporous shell of the silica template; d) a  
7 hollow morphology that entails a uniform thin carbon layer (thickness  $\sim 50 \text{ nm}$ )  
8 greatly reducing diffusion distances and e) the existence of graphitic domains  
9 enhancing their electronic conductivity. The combination of all these chemical  
10 and structural properties guarantees a large number of highly active and fully  
11 accessible catalytic sites and rapid mass-transfer kinetics. Consequently, our  
12 electrocatalyst exhibits a high ORR activity - which is close to or higher than  
13 that of the Pt/C catalyst - in both basic and acid media. It is worth noting that the  
14 excellent electrocatalytic activity has been confirmed by using a rotating ring-  
15 disk electrode, which has allowed assessing the reaction mechanism and  
16 quantifying the percentage of harmful  $\text{H}_2\text{O}_2$  produced, a procedure not widely  
17 used in the literature.<sup>19, 21-23</sup> Furthermore, an alkaline fuel cell (AAEMFC) has  
18 been successfully assembled with the Fe-N-doped cathode catalyst.

## 39 **Results and discussion**

### 43 **Structural and chemical properties of the N-doped carbon capsules**

46 An illustration of the synthetic method is shown in Figure 1. In order to  
47 synthesize porous hollow carbon particles, we used as template silica particles  
48 with a structure formed by a solid core and a mesoporous shell, and pyrrole as  
49 carbon precursor and N-dopant. The pores of the silica particles were  
50 impregnated with  $\text{FeCl}_3$  and, then, infiltrated with pyrrole vapors which rapidly  
51 polymerized to polypyrrole. Subsequently, the silica-polypyrrole composite was  
52  
53  
54  
55  
56  
57  
58  
59  
60

1  
2  
3 carbonized and the silica framework and most of iron were dissolved with  
4 hydrofluoric acid, giving rise to Fe-N-doped carbon capsules (Fe-N-CC).  
5  
6  
7

8 The SEM image in Figure 2a shows that the carbon particles have a  
9 spherical morphology with a uniform diameter of  $580 \pm 40$  nm (see inset in  
10 Figure 2a). These microspheres exhibit a hollow structure, as evidenced by the  
11 high-magnification TEM image displayed in Figure 2b, which reveals that the  
12 diameter of the central macroporous core is around  $330 \pm 40$  nm with a porous  
13 shell of around 50 nm thick. These carbon particles exhibit a high BET  
14 (Brunauer–Emmett–Teller) surface area of  $1590 \text{ m}^2 \text{ g}^{-1}$  and a large pore volume  
15 of  $1.46 \text{ cm}^3 \text{ g}^{-1}$  (see Table 1). Importantly, the porosity of the carbon layer is  
16 made up almost exclusively of mesopores, as calculated by means of the  $\alpha_s$ -  
17 plot method applied to the  $\text{N}_2$  adsorption branch (see inset in Figure 2c), with  
18 the micropores representing only  $< 5$  % of the total pore volume (Table 1).  
19 These mesopores have a uniform size centered at around 3.8 nm, as deduced  
20 by the Kruk-Jaroniec-Sayari (KJS) method applied to the  $\text{N}_2$  isotherm  
21 adsorption branch (Figure S1).  
22  
23  
24  
25  
26  
27  
28  
29  
30  
31  
32  
33  
34  
35  
36  
37  
38  
39

40 The microstructure of the Fe-N-CC sample was investigated by X-ray  
41 diffraction (XRD). A sharp peak can be observed at  $2\theta = 26^\circ$ , which  
42 corresponds to the (002) diffraction peak of graphite (see Figure S2a). This  
43 peak is superimposed on a broad profile corresponding to amorphous carbon,  
44 suggesting the presence of a certain amount of graphitized carbon embedded in  
45 an amorphous carbon matrix. The presence of these graphitic domains is  
46 attributable to the iron nanoparticles generated during the high temperature  
47 treatment (derived from the  $\text{FeCl}_3$  used for the oxidative polymerization of  
48 pyrrole), which act as a graphitization catalyst during the carbonization,  
49  
50  
51  
52  
53  
54  
55  
56  
57  
58  
59  
60

1  
2  
3 converting a certain amount of amorphous carbon into graphitic  
4 nanostructures.<sup>39-41</sup> No peaks attributable to Fe/Fe<sub>3</sub>C nanoparticles can be  
5 observed, whereas the XRD pattern of the sample before the harsh acid  
6 washing showed the presence of a small amount of metal Fe and Fe<sub>3</sub>C (see  
7 Figure S2b). The existence of the graphitic domains was further confirmed by  
8 Raman spectroscopy performed in randomly selected regions. Thus, as can be  
9 seen in Figure S2c, the Raman spectrum corresponding to an amorphous  
10 carbon region is composed of two broad overlapping D and G bands ( $I_D/I_G =$   
11 1.14, FWHM of G band = 68 cm<sup>-1</sup>), whereas that of the graphitic carbon regions  
12 exhibits a high-intensity sharp G band at 1575 cm<sup>-1</sup> and a weak D band at 1350  
13 cm<sup>-1</sup> ( $I_D/I_G = 1.2$ , FWHM of G band = 37 cm<sup>-1</sup>) associated to defects in the  
14 graphitic sp<sup>2</sup> carbon structures. The amount of graphitic carbon in the Fe-N-CC  
15 sample is around 10 wt %, as deduced by means of thermogravimetric analysis  
16 (see Figure S2d). The electrical conductivity of the Fe-N-CC sample is 22 S m<sup>-1</sup>  
17 (see Table 1). This good value of conductivity can be attributed to the  
18 combination of N-doping and the presence of a certain amount of graphitic  
19 domains.

20  
21  
22  
23  
24  
25  
26  
27  
28  
29  
30  
31  
32  
33  
34  
35  
36  
37  
38  
39  
40  
41 The bulk nitrogen content of the Fe-N-CC sample -as determined by  
42 elemental analysis- is 5.88 wt % (Table 1). The analysis of the chemical nature  
43 of the nitrogen groups inserted within the carbon framework was performed  
44 through X-ray photoelectron spectroscopy (XPS) (Figure 2d). The high-  
45 resolution N 1s XPS spectrum can be deconvoluted in two main peaks at 398.6  
46 and 400.9 eV, which are assigned respectively to pyridinic-N (N-6; 40.4%) and  
47 quaternary-N (N-Q; 53.7%), and a minor peak at 402.7 eV, which can be  
48 attributed to pyridine-N-oxides (N-O; 5.9 %).<sup>42, 43</sup> The N/C atomic ratios  
49  
50  
51  
52  
53  
54  
55  
56  
57  
58  
59  
60



1  
2  
3 corresponding to the bulk -elemental analysis- (0.064) and the surface -XPS  
4 analysis- (0.068) (see Figure S3a) of the particles are similar, indicating that the  
5 nitrogen functionalities are homogeneously distributed throughout the particles.  
6  
7 The XPS general spectrum in Figure S3a further evidences the presence of a  
8 small amount of Fe (~710 eV). Specifically, 0.2 at % Fe remains after four days  
9 of harsh acid washing with HF (48 %) which reveals the high chemical stability  
10 of the Fe-N-doped carbon capsules. ICP analysis also shows a bulk iron  
11 content of 0.2 at % (~ 0.7 wt %). Deconvolution of the high-resolution Fe 2p<sub>3/2</sub>  
12 XPS spectrum (Figure S3b) hints at the presence of iron coordinated to  
13 nitrogen, but no Fe<sub>3</sub>C can be detected (see further discussion in SI), both of  
14 which have been shown to be active in ORR.<sup>44, 45</sup> However, taking into account  
15 that only traces of iron are present, it is hard to accurately analyze the iron  
16 species by XPS (detection limit ~ 0.1-0.2 at %). Therefore, in order to get more  
17 insights into the kind of iron species present in the material, TEM/HRTEM  
18 studies were performed. The EDX-TEM mapping images in Figure S4 show that  
19 C, N, O and Fe in the Fe-N-CC sample are homogeneously distributed. It must  
20 be noted that no nanoparticles containing iron species are observable in the  
21 capsules in the TEM picture in Figure S4a, but EDX shows that this element is  
22 homogeneous distributed within the carbon framework. Further analysis was  
23 therefore performed by calculating the EDX concentration profiles of N and Fe  
24 along the line drawn on these carbon capsules (see Figure 3a). As can be seen  
25 in Figure 3b, the iron and nitrogen profiles perfectly correlate with each other,  
26 suggesting that the iron atoms are coordinated to nitrogen (Fe-N<sub>x</sub>). However,  
27 this is not the only iron species found by HRTEM. As revealed by Figure S5a,  
28 Fe<sub>3</sub>C nanoparticles are found encapsulated by a graphitic layer. A closer look at  
29  
30  
31  
32  
33  
34  
35  
36  
37  
38  
39  
40  
41  
42  
43  
44  
45  
46  
47  
48  
49  
50  
51  
52  
53  
54  
55  
56  
57  
58  
59  
60

1  
2  
3 these nanoparticles reveals that they are coated by a graphitic carbon layer of  
4  
5 around 15 nm (see Figure S5b), with an interlayer spacing of 0.336 nm,  
6  
7 corresponding to the (002) plane of graphitic carbon. As shown in Figures S5c  
8  
9 and S5d for a typical nanoparticle, the spacing of the crystalline lattices in two  
10  
11 directions was 0.236 nm and 0.200 nm, which are incompatible with the iron  
12  
13 phases, but can be assigned to Fe<sub>3</sub>C phase. It should be noted that the Fe<sub>3</sub>C  
14  
15 particles constitute a minor amount as deduced by TEM inspection. The  
16  
17 presence of a graphitic layer surrounding Fe<sub>3</sub>C explains why those particles are  
18  
19 not detected by XPS, whose analysis depth is < 10 nm, and also why they are  
20  
21 not removed after acid washing. It must be pointed out that, in order to test the  
22  
23 reproducibility of this procedure, the synthesis was repeated several times. In all  
24  
25 the cases, the chemical and the textural properties of the Fe-N-doped carbon  
26  
27 capsules were similar.  
28  
29  
30  
31  
32  
33

### 34 **Electrocatalytic performance of the N-doped carbon capsules in the** 35 **oxygen reduction reaction (ORR)** 36

37  
38 The electrocatalytic activity of the Fe-N-doped carbon capsules towards  
39  
40 ORR was assessed in both acidic and alkaline electrolytes. The ORR activity  
41  
42 was first studied in a three-electrode cell configuration by using cyclic  
43  
44 voltammetry in N<sub>2</sub>- and O<sub>2</sub>-saturated 0.1 M KOH and 0.5 M H<sub>2</sub>SO<sub>4</sub> solutions.  
45  
46 Figures S6a and S6b show the CV curves of Fe-N-CC in N<sub>2</sub>- and O<sub>2</sub>-saturated  
47  
48 electrolytes at a scan rate of 100 mV s<sup>-1</sup>. In both cases, featureless  
49  
50 voltammetric curves are observed in the N<sub>2</sub>-saturated solution. The  
51  
52 voltammograms only exhibit capacitive charging currents associated with the  
53  
54 surface area of the particles and pseudocapacitive currents attributable to the  
55  
56  
57  
58  
59  
60

1  
2  
3 N- and O- groups.<sup>46</sup> In contrast, when the electrolyte is saturated with O<sub>2</sub>, a  
4 well-defined cathodic peak is observed at around 0.82 V in KOH (see Figure  
5 S6a) and 0.58 V in H<sub>2</sub>SO<sub>4</sub> (see Figure S6b), which suggests pronounced ORR  
6 electrocatalytic activity. The value of peak potential obtained in basic medium is  
7 shifted to positive values when compared to some of the top-performing N-  
8 doped carbon materials that can be found in the literature.<sup>22, 47-51</sup> These results  
9 highlight the outstanding electrocatalytic performance of Fe-N-CC, which may  
10 be attributable to a synergetic effect between N- and Fe-doping. Taking into  
11 account that carbon materials are less active in acid than in alkaline medium,<sup>2</sup>  
12 the pronounced cathodic peak found in 0.1 M KOH is less sharp in 0.5 M  
13 H<sub>2</sub>SO<sub>4</sub>. Nevertheless, it is still noticeable compared to other catalysts that can  
14 be found in the literature,<sup>52-54</sup> which suggests also good catalytic activity in acid  
15 medium.  
16  
17  
18  
19  
20  
21  
22  
23  
24  
25  
26  
27  
28  
29  
30  
31

32 A detailed investigation of the mass-transfer kinetics and electrochemical  
33 performance of the Fe-N-CC sample was carried out by experiments performed  
34 using a rotating disk electrode (RDE) and a rotating ring-disk electrode (RRDE).  
35 The polarization curves obtained from RDE (1600 rpm) linear sweep  
36 voltammetry in O<sub>2</sub>-saturated 0.5 M H<sub>2</sub>SO<sub>4</sub> and 0.1 M KOH are shown in Figures  
37 4a and 4b, respectively. To provide a realistic picture, the results are compared  
38 with those of a commercial Pt/C catalyst (20 wt % Pt) using the same amount of  
39 each catalyst (0.1 mg cm<sup>-2</sup>). In 0.1 M KOH, the ORR polarization curve of Fe-N-  
40 CC exhibits a high onset (*ca.* 0.94 V) and half-wave potentials (*ca.* 0.83 V), both  
41 values being higher than those of Pt/C (*ca.* 0.93 V and *ca.* 0.78 V respectively).  
42 A comparison of the value of onset potential of Fe-N-CC with that of state-of-  
43 the-art N-doped and Fe-N-doped carbon materials evidences the outstanding  
44  
45  
46  
47  
48  
49  
50  
51  
52  
53  
54  
55  
56  
57  
58  
59  
60

1  
2  
3 activity offered by Fe-N-CC in basic medium (see Table S1). On the other hand,  
4  
5 in 0.5 M H<sub>2</sub>SO<sub>4</sub>, the Fe-N-CC sample possesses a similar onset potential (0.80  
6  
7 V) to that of Pt/C (ca. 0.80 V, comparable to that found by other authors for  
8  
9 analogous mass loading<sup>36, 55</sup>), although the half-wave potential is slightly  
10  
11 decreased (ca. 0.52 V vs. 0.60 for Pt/C).<sup>36</sup> This value of onset potential is  
12  
13 comparable to the best N- and Fe-N-doped carbon catalysts reported so far in  
14  
15 the literature (see Table S2). Especially remarkable is the behavior in basic  
16  
17 medium in which the diffusion-limited current density is significantly improved  
18  
19 (by 10 %) in relation to Pt/C (Note that the mass loadings of both catalyst are  
20  
21 the same, 0.1 mg cm<sup>-2</sup>) and superior to many advanced N-doped and Fe-N  
22  
23 doped carbon catalysts reported in the literature.<sup>48, 56-58</sup> It is worth noting that  
24  
25 the value of diffusion-limited current density measured for commercial Pt/C is in  
26  
27 agreement with other reported values for the same mass loading of catalyst.<sup>22,  
28  
29  
30  
31  
32 23, 47, 59</sup>

33  
34  
35 The ORR kinetics in acidic and alkaline media was also assessed by  
36  
37 using the Koutecky-Levich equation. The rotation dependent currents in Figures  
38  
39 S7a-S7b show a linear reciprocal square-root relationship according to the  
40  
41 Koutecky-Levich plot (see Figure S7c-S7d), with a slope more similar to an  
42  
43 ideal four-electron process than to an ideal two-electron process. More  
44  
45 specifically, in 0.1 M KOH, the number of electrons thus calculated is 3.7 at 0.58  
46  
47 V (see Figure S7c). This result suggests that Fe-N-CC catalyzes the direct four-  
48  
49 electron oxygen reduction reaction to OH<sup>-</sup>. The calculated electrochemical  
50  
51 kinetic current density ( $J_K$ ) value of 18.3 mA cm<sup>-2</sup> at 0.58 V is more than three  
52  
53 times higher than that of commercially available Pt/C (5 mA cm<sup>-2</sup> at 0.58 V,  
54  
55 value similar to those reported in the literature for the same mass loading of  
56  
57  
58  
59  
60

1  
2  
3 Pt/C<sup>47, 59</sup>) in basic medium. Furthermore, this value is superior to that of many  
4  
5 nitrogen and Fe-N doped carbons found in the literature (see Table S1). In  
6  
7 acidic medium, Fe-N-CC also catalyzes the four-electron process (see Figure  
8  
9 S7d) with a  $J_K$  value of 4.85 mA cm<sup>-2</sup> at 0.46 V, still superior to commercial Pt/C  
10  
11 (4 mA cm<sup>-2</sup>, value again comparable to the literature<sup>60</sup>). These results reveal the  
12  
13 high electrocatalytic activity towards ORR compared to Pt/C.  
14  
15

16  
17 A more in-depth study of the reaction pathway was performed with a  
18  
19 RRDE, in which the amount of HO<sub>2</sub><sup>-</sup> can be accurately determined. Figures 4c-  
20  
21 4d provide a comparison of the number of electrons transferred along with the  
22  
23 yield of peroxide formed for the Fe-N-CC carbon capsules and Pt/C in 0.1 M  
24  
25 KOH and 0.5 M H<sub>2</sub>SO<sub>4</sub> electrolytes. The Fe-N-CC sample shows an  $n$  value  
26  
27 higher than 3.8 in basic medium and the HO<sub>2</sub><sup>-</sup> formation is lower than 10 % over  
28  
29 the whole range of potentials, demonstrating its excellent electrocatalytic  
30  
31 selectivity. In acidic medium, the H<sub>2</sub>O<sub>2</sub> yield is even lower, *i.e.* < 8 %, while the  
32  
33 number of electrons transferred is kept at ~ 3.8 (see Figure 4d). These results  
34  
35 clearly indicate that ORR on Fe-N-CC carbon proceeds *via* the efficient four-  
36  
37 electron pathway.<sup>61</sup> This is very important from an operation point of view, as  
38  
39 the H<sub>2</sub>O<sub>2</sub> produced on the two-electron process may degrade the catalyst layer  
40  
41 and the membrane.<sup>62</sup>  
42  
43  
44  
45

46  
47 With the aim of assessing the role of iron on creating ORR catalytic active  
48  
49 sites, we investigated the ORR activity of Fe-N-CC in 0.1 M KOH containing 10  
50  
51 mM KCN. It is well known that CN<sup>-</sup> ions can coordinate strongly to iron and,  
52  
53 therefore, poison the iron-centered catalytic sites for ORR,<sup>63</sup> whereas the  
54  
55 nitrogen active centers are inert to CN<sup>-</sup> ions.<sup>64</sup> As can be seen in Figure 5, the  
56  
57 addition of KCN negatively shifts the onset and half-wave potentials respectively  
58  
59  
60

1  
2  
3 by ~ 57 and ~ 60 mV. In addition, a 16 % decrease is recorded on the diffusion  
4 limited current. These results show that part of the activity of the Fe-N-doped  
5 carbon capsules is indeed attributable to the Fe-N coordination sites identified  
6 in the capsules (*vide supra*). Contribution of the Fe<sub>3</sub>C phase can be discarded  
7 taking into account that it is encapsulated in a graphitic carbon layer which does  
8 not allow penetration of the electrolyte. Anyway, Figure 5 also proves that the  
9 catalytic activity of the N-sites is not negligible at all. In fact, the Fe-N-carbon  
10 catalyst poisoned with CN<sup>-</sup> exhibits a limiting current density which is just ~ 8 %  
11 lower than that of commercial Pt/C and an onset potential of 0.89 V.  
12 Furthermore, these values are still higher or comparable to those of many top-  
13 performing metal-free N-doped carbons.<sup>48, 54, 59, 65, 66</sup> Indeed, the carbon  
14 particles contain a great number of active sites (N-groups) that are well-  
15 distributed along a large surface area, thereby providing numerous catalytic  
16 centers for O<sub>2</sub> chemisorption and reduction.<sup>67, 68</sup> Importantly, most of the N-  
17 groups correspond to quaternary and pyridinic nitrogen, which are the two main  
18 contributors to the electrocatalytic activity.<sup>13, 69</sup> Summarizing, the above results  
19 clearly show that there are two types of active sites coexisting in the Fe-N-  
20 carbon capsules catalysts, *i.e.* Fe-N and N. Besides, the carbon particles exhibit  
21 an optimized pore structure made up of uniform mesopores of ca. 4 nm and  
22 short diffusional paths arising from an effective particle size ~ 50 nm, which  
23 ensure fast mass-transfer processes and maximize exposure of the nitrogen  
24 and iron active sites to the reactants/electrolyte enhancing their utilization.<sup>70</sup>

25  
26  
27  
28  
29  
30  
31  
32  
33  
34  
35  
36  
37  
38  
39  
40  
41  
42  
43  
44  
45  
46  
47  
48  
49  
50  
51  
52  
53 The long-term stability of ORR catalysts is also a major concern in fuel-cell  
54 technology and, therefore, much attention has been paid recently to this  
55 feature.<sup>6</sup> Accordingly, the durability of the Fe-N-CC catalyst was tested following  
56  
57  
58  
59  
60

1  
2  
3 a US Department of Energy's accelerated durability test protocol based on  
4 cycling the catalysts between 0.6 and 1.0 V (vs. RHE) at  $50 \text{ mV s}^{-1}$  under  $\text{N}_2$   
5 atmosphere in 0.1 M KOH and 0.5 M  $\text{H}_2\text{SO}_4$ .<sup>27, 31</sup> Figures 6a-6b compare the  
6 linear sweep voltammetry curves at a rotation speed of 1600 rpm in  $\text{O}_2$ -  
7 saturated electrolyte before and after the accelerated durability test in KOH and  
8  $\text{H}_2\text{SO}_4$  electrolytes. In KOH, the Fe-N-CC catalyst exhibits a remarkable  
9 durability performance, in which the onset potential decreases by only  $\sim 20 \text{ mV}$   
10 after 3500 cycles, with no appreciable variation in the half-wave potential. On  
11 the contrary, commercial Pt/C exhibits a decrease of the onset and half-wave  
12 potentials of 10 and 90 mV respectively. Chronoamperometric testing was  
13 carried out to confirm the durability of the nitrogen-doped carbon capsules and  
14 commercial Pt/C in 0.1 M KOH. The results shown in Figure S8 reveal that the  
15 Fe-N-CC sample retains *ca.* 90 % of the initial current after 10,000 s, whereas  
16 commercial Pt/C retains only 70 % of the initial current. In  $\text{H}_2\text{SO}_4$ , after 3500  
17 continuous cycles, the half-wave potential of Fe-N-CC shows a negative shift of  
18  $\sim 40 \text{ mV}$  and the onset potential slightly decreases from 0.80 V to 0.76 V (see  
19 Figure 6b). These values show improved resistance to performance decay  
20 when compared to Pt/C, which suffers a decrease of 70 mV on the onset  
21 potential and 140 mV on the half-wave potential. These results prove the  
22 robustness of the Fe-N and N catalytic sites regardless of the electrolyte used,  
23 which was already suggested by their resistance to the harsh acid washing.  
24  
25  
26  
27  
28  
29  
30  
31  
32  
33  
34  
35  
36  
37  
38  
39  
40  
41  
42  
43  
44  
45  
46  
47  
48  
49

50 One of the disadvantages of platinum-based electrocatalysts in direct  
51 methanol fuel cells (DMFC), is methanol crossover from the anode to the  
52 cathode.<sup>71</sup> To analyze this issue, the chronoamperometric response was  
53 measured by injecting methanol into the  $\text{O}_2$ -saturated 0.1 M KOH electrolyte  
54  
55  
56  
57  
58  
59  
60

1  
2  
3 (see Figure 6c). Both Fe-N-CC and Pt/C catalysts show ORR activity when  
4 oxygen is bubbling. However, after the injection of methanol ( $t = 160$  s), a  
5 dramatic loss of cathodic current is registered in the platinum catalyst, indicating  
6 rapid degradation of its ORR activity.<sup>25, 72</sup> In contrast, Fe-N-CC catalyst does not  
7 show any sensitivity towards the presence of methanol, the cathodic current  
8 remaining relatively stable after methanol injection. Similar results were  
9 obtained in acid medium. Thus, Fe-N-CC electrocatalyst shows excellent  
10 tolerance to methanol crossover with an equally good ORR performance with or  
11 without methanol (see Figure 6d). These results clearly show that the Fe-N-  
12 doped carbon particles constitute an outstanding catalyst in the ORR process  
13 regardless of the type of electrolyte or fuel used.  
14  
15  
16  
17  
18  
19  
20  
21  
22  
23  
24  
25  
26  
27

### 28 **Alkaline anion exchange membrane fuel cell (AAEMFC) assembly**

29  
30  
31 The real applicability of the Fe-N-CC catalyst was assessed by using with  
32 Fe-N-CC and Pt/C as cathode catalysts in AAEMFC. The polarization curves in  
33 Figure 7 show that commercial Pt/C performs better than Fe-N-CC at low  
34 current density ( $< 100 \text{ mA cm}^{-2}$ ), but worse at high current density. However,  
35 overall, Fe-N-CC produces a higher power density than Pt/C. EIS analysis was  
36 carried out to determine the exact contribution of the catalyst with respect to  
37 other factors, such as Ohmic resistance and mass transport, to the overall  
38 performance of the cell. Half-cell impedance spectra of the anode and cathode,  
39 in addition to the whole cell, were also measured. Figure S9 shows the Nyquist  
40 plots corresponding to the cathode and the whole cell measurements at various  
41 current densities. The contribution from the anode is insignificant in all cases,  
42 especially at low current density. Therefore, it can be assumed that cathode  
43 kinetics are the dominant factor affecting the overall performance. Regardless  
44  
45  
46  
47  
48  
49  
50  
51  
52  
53  
54  
55  
56  
57  
58  
59  
60



1  
2  
3 of the current density, the charge transfer resistance of Fe-N-CC is significantly  
4  
5 lower than that of Pt/C, which confirms the RDE results. However, the low  
6  
7 charge transfer resistance shown by the EIS measurements is not reflected in  
8  
9 an improved performance in the polarization curve at low current densities as  
10  
11 shown by Figure 7. This is mainly due to the lower starting potential (0.96 V vs.  
12  
13 1.01 V) of the Fe-N-CC fuel cell at open circuit voltage (OCV). The low OCV  
14  
15 could be caused by other reasons such as mixed potential or gas crossover.<sup>62</sup>  
16  
17 <sup>73</sup> However, as more current is drawn from the fuel cell, the improved  
18  
19 performance expected from the EIS and RDE measurements manifests itself in  
20  
21 lower voltage losses compared to Pt/C. These results suggest that Fe-N-CC  
22  
23 could serve as a good substitute for Pt/C as cathode catalyst. Improvements in  
24  
25 the CCM fabrication method would further enhance the fuel cell performance.  
26  
27  
28  
29

## 30 **Conclusions**

31  
32  
33 In summary, a highly efficient ORR iron and nitrogen doped hollow carbon  
34  
35 electrocatalyst has been synthesized using the nanocasting approach and  
36  
37 pyrrole as N-rich carbon precursor. The resulting carbon particles possess iron  
38  
39 traces mainly in the form of Fe-N coordination sites (~ 0.7 wt %) and a high  
40  
41 content of nitrogen moieties (~ 6 wt %) comprising mainly quaternary and  
42  
43 pyridinic groups. The structure of these hollow particles consists of a highly  
44  
45 porous ( $S_{\text{BET}} \sim 1500 \text{ m}^2 \text{ g}^{-1}$ ), curved, thin carbon layer (thickness ~ 50 nm)  
46  
47 containing pores with a size centered at around 4 nm. This remarkable  
48  
49 combination of chemical and structural properties gives rise to an active ORR  
50  
51 electrocatalyst with numerous and easily accessible catalytic centers.  
52  
53  
54  
55  
56 Importantly, it has been shown that both N-sites and Fe-N coordination sites are  
57  
58  
59  
60

1  
2  
3 contributing to the catalytic activity. Thereby, the Fe-N-doped hollow carbon  
4  
5 particles exhibit an outstanding activity in basic media and an excellent  
6  
7 (comparable to Pt/C) performance in acidic media, with a peroxide yield lower  
8  
9 than 10 %, an electron transfer number close to 4, and onset and half-wave  
10  
11 potentials superior (basic media) or similar (acid media) to those of commercial  
12  
13 Pt/C. Furthermore, these nitrogen-doped carbon capsules with iron traces  
14  
15 exhibit an excellent resistance to methanol crossover and a superior long-term  
16  
17 durability, beating the platinum supported carbon in both electrolytes (*i.e.* KOH  
18  
19 and H<sub>2</sub>SO<sub>4</sub>). The practical applicability of the Fe-N-doped catalyst has been  
20  
21 shown by assembling an AAEMFC with a performance matching that of another  
22  
23 AAEMFC based on a Pt/C cathode catalyst.  
24  
25  
26

## 27 28 **Experimental Section**

### 29 30 31 **Preparation of mesoporous Fe-N-doped carbon capsules**

32  
33 The N-doped carbon capsules were fabricated as reported first by our group.<sup>46</sup>  
34  
35 Briefly, silica particles with a hollow core and a mesoporous shell (SCMS) were  
36  
37 synthesized as reported by Unger *et al.*<sup>74</sup> Afterwards, the SCMS particles were  
38  
39 impregnated by the drop-wise impregnation technique with a 2 M FeCl<sub>3</sub> ethanol  
40  
41 solution (around 0.27 g FeCl<sub>3</sub> / g silica). Then, the impregnated sample was  
42  
43 exposed to pyrrole (Aldrich, 99%) vapors at 25 °C for 22 h in a closed vessel.  
44  
45 The dark solid thus obtained was heated under N<sub>2</sub> to 850 °C (3 °C min<sup>-1</sup>) for 1 h.  
46  
47 Finally, the carbonized composite was treated with hydrofluoric acid for four  
48  
49 days to dissolve the silica framework. The carbon residue was collected by  
50  
51 filtration, washed with distilled water, and dried at 120 °C for several hours. The  
52  
53  
54  
55  
56  
57  
58  
59  
60

1  
2  
3 carbon capsules with nitrogen functionalities have been designated as *Fe-N-*  
4  
5 CC.  
6  
7

### 8 **Characterization of materials**

9

10  
11 The morphology of the powders was examined by scanning (SEM, Zeiss DSM  
12 942) and transmission (HRTEM, JEOL (JEM 2100-F)) electron microscopy.  
13  
14 Nitrogen sorption isotherms were performed at -196 °C in a Micromeritics ASAP  
15 2020 volumetric adsorption system. The Brunauer-Emmett-Teller (BET) surface  
16  
17 area was deduced from an analysis of the isotherm in the relative pressure  
18  
19 range of 0.04-0.20. The total pore volume was calculated from the amount of  
20  
21 nitrogen adsorbed at a relative pressure of 0.90. The mesopore size distribution  
22  
23 was calculated by means of the Kruk-Jaroniec-Sayari (KJS) method.<sup>75</sup> The  
24  
25 primary mesopore volume ( $V_m$ ) and external surface area ( $S_{ext}$ ) were estimated  
26  
27 using the  $\alpha_s$ -plot method. The reference adsorption data used for the  $\alpha_s$  analysis  
28  
29 of the carbon sample correspond to a non-graphitized carbon black sample.<sup>76</sup>  
30  
31  
32  
33  
34  
35

36 The thermogravimetric analysis was performed on a CI Electronics system.  
37  
38 Raman spectra were recorded on a Horiva (LabRamHR-800) spectrometer. The  
39  
40 source of radiation was a laser operating at a wavelength of 514 nm and at a  
41  
42 power of 25 mW. Calculation of the parameters  $I_D/I_G$  (integrated intensity ratio)  
43  
44 and width at half maximum (FWHM) of the G band was done by the  
45  
46 deconvolution of the spectra. The curve fitting was performed with the  
47  
48 combination of Gaussian-Lorentzian line shaped that gave the minimum fitting  
49  
50 error. X-ray photoelectron spectroscopy (XPS) was performed on a Specs  
51  
52 spectrometer, using Mg K $\alpha$  (1253.6 eV) radiation from a double anode at 150  
53  
54 W. Binding energies for the high resolution spectra were calibrated by setting C  
55  
56  
57  
58  
59  
60

1  
2  
3 1s to 284.4 eV. X-ray diffraction (XRD) patterns were obtained on a Siemens  
4 D5000 instrument operating at 40 kV and 20 mA and using Cu K $\alpha$  radiation  
5 ( $\lambda=0.15406$  nm). Bulk elemental analysis (C, H, N and O) of the samples was  
6 carried out on a LECO CHN-932 microanalyzer. The bulk Fe content in the  
7 catalysts was obtained by ICP-MS analysis in a 7700x equipment (Agilent).  
8  
9

10  
11  
12 The electrical conductivity of the carbon materials was determined by pressing  
13 the powdered material at 7.1 MPa.  
14

### 15 16 17 18 19 20 **Electrochemical measurements**

21  
22  
23 Electrochemical measurements were conducted using an AUTOLAB PGSTAT  
24 101 and a Multi AUTOLAB M101 (CH Instruments). Fe-N-CC catalyst inks were  
25 prepared by ultrasonically dispersing 1.5 mg of Fe-N-CC catalyst in a solution  
26 containing 100  $\mu$ L Nafion (5 wt %) solution and 900  $\mu$ L deionized water. For  
27 comparison, the Pt/C catalyst (20 wt % Pt on graphitized carbon, Sigma-Aldrich)  
28 ink was prepared in the same way, using the same amount of catalyst (*i.e.* 1.5  
29 mg). The mass loading of both catalysts is the same, *i.e.* 0.1 mg cm<sup>-2</sup>. The  
30 above prepared catalyst inks were deposited onto a polished glassy carbon  
31 electrode ( $\alpha$ -Al<sub>2</sub>O<sub>3</sub> slurry, 50 nm) and dried under room temperature. A  
32 conventional three-electrode cell was employed, incorporating Ag/AgCl (3 M  
33 KCl) as the reference electrode, a Pt wire as the counter electrode and a  
34 rotating disk electrode (RDE) or rotating ring-disk electrode (RRDE) coated with  
35 the catalyst film as the working electrode. The electrolyte was 0.5 M H<sub>2</sub>SO<sub>4</sub>  
36 solution or 0.1 M KOH solution. All the experiments were carried out at 20 °C.  
37  
38  
39 Before testing, O<sub>2</sub>/N<sub>2</sub> gas was bubbled through the electrolyte in the cell for 30  
40 min to saturate it with O<sub>2</sub>/N<sub>2</sub>. The measured potentials vs. Ag/AgCl (3 M KCl)  
41  
42  
43  
44  
45  
46  
47  
48  
49  
50  
51  
52  
53  
54  
55  
56  
57  
58  
59  
60

1  
2  
3 were converted to the reversible hydrogen electrode (RHE) scale according to  
4  
5 the Nernst equation:

$$E_{\text{RHE}} = E_{\text{Ag/AgCl}} + 0.059 \text{ pH} + E_{\text{Ag/AgCl}}^{\circ} \quad (1)$$

6  
7  
8  
9 where  $E_{\text{Ag/AgCl}}$  is the experimentally measured potential vs. Ag/AgCl reference  
10  
11 and  $E_{\text{Ag/AgCl}}^{\circ} = 0.21 \text{ V}$  at 20 °C. The values of potential provided along the text  
12  
13 are referenced against RHE unless otherwise stated.  
14  
15

16  
17 Cyclic voltammetry (CV) was performed from 0 to 1.2 V vs. RHE in O<sub>2</sub>-  
18  
19 and N<sub>2</sub>-saturated 0.1 M KOH and 0.5 M H<sub>2</sub>SO<sub>4</sub> electrolytes, with a sweep rate  
20  
21 of 100 mV s<sup>-1</sup>.  
22

23  
24 RDE linear sweep voltammetry (LSV) measurements were conducted  
25  
26 from 1.2 to 0 V vs. RHE in O<sub>2</sub>-saturated 0.1 M KOH and 0.5 M H<sub>2</sub>SO<sub>4</sub>  
27  
28 electrolytes at a scan rate of 10 mV s<sup>-1</sup> under disk rotation rates of 400, 800,  
29  
30 1200, 1600, 2000 and 2400 rpm. The working electrode was a 3.0 mm diameter  
31  
32 GC rotating disk electrode.  
33

34  
35 The apparent number of electrons transferred during ORR on the carbon  
36  
37 catalysts was determined by the Koutechy-Levich equation given by:

$$\frac{1}{J} = \frac{1}{J_L} + \frac{1}{J_K} = \frac{1}{B\omega^{1/2}} + \frac{1}{J_K} \quad (2)$$

$$B = 0.62nFC_0(D_0)^{2/3}\nu^{1/6} \quad (3)$$

38  
39  
40  
41  
42  
43 where  $J$  is the measured current density,  $J_K$  is the kinetic current density,  $J_L$  is  
44  
45 the diffusion-limited current density,  $\omega$  is the electrode rotation rate,  $F$  is the  
46  
47 Faraday constant (96485 C mol<sup>-1</sup>),  $C_0$  is the bulk concentration of O<sub>2</sub> (1.1 × 10<sup>-3</sup>  
48  
49 mol L<sup>-1</sup> for 0.5 M H<sub>2</sub>SO<sub>4</sub> solution and 1.2 × 10<sup>-3</sup> mol L<sup>-1</sup> 0.1 M KOH solution),  $D_0$   
50  
51 is the diffusion coefficient of O<sub>2</sub> (1.4 × 10<sup>-5</sup> cm<sup>2</sup> s<sup>-1</sup> for 0.5 M H<sub>2</sub>SO<sub>4</sub> solution and  
52  
53 1.9 × 10<sup>-5</sup> cm<sup>2</sup> s<sup>-1</sup> for 0.1 M KOH solution) and  $\nu$  is the kinetic viscosity of the  
54  
55  
56  
57  
58  
59  
60

1  
2  
3 electrolyte ( $0.01 \text{ cm}^2 \text{ s}^{-1}$  for both  $0.5 \text{ M H}_2\text{SO}_4$  solution and  $0.1 \text{ M KOH}$   
4 solution).<sup>77-79</sup>

5  
6  
7 For the RRDE tests, the disk potential was scanned at  $10 \text{ mV s}^{-1}$ , while  
8 the ring potential was held at  $1.5 \text{ V vs. RHE}$  in order to oxidize any  $\text{H}_2\text{O}_2$   
9 produced.<sup>8, 80</sup> The working electrode was a  $5 \text{ mm GC}$  disk electrode and a  $\text{Pt}$   
10 ring electrode ( $375 \text{ }\mu\text{m}$  gap). The  $\text{H}_2\text{O}_2$  collection efficiency at the ring  
11 ( $N=0.249$ ) was provided by the manufacturer. The following equations were  
12 used to calculate  $n$  (the apparent number of electrons transferred during ORR)  
13 and  $\% \text{ H}_2\text{O}_2$  (the percentage of  $\text{H}_2\text{O}_2$  released during ORR):<sup>81</sup>

$$n = \frac{4 I_D}{I_D + (I_R/N)} \quad (4)$$

$$\% \text{ H}_2\text{O}_2 = 100 \frac{2 I_R/N}{I_D + (I_R/N)} \quad (5)$$

14  
15  
16 where  $I_D$  is the Faradaic current at the disk,  $I_R$  is the Faradaic current at the ring,  
17  
18  
19  $N$  is the  $\text{H}_2\text{O}_2$  collection coefficient at the ring.

20  
21  
22 The stability of the catalyst was assessed by means of an US  
23  
24  
25  
26  
27  
28  
29  
30  
31  
32  
33  
34  
35  
36  
37  
38  
39  
40  
41  
42  
43  
44  
45  
46  
47  
48  
49  
50  
51  
52  
53  
54  
55  
56  
57  
58  
59  
60  
Department of Energy's accelerated durability test protocol by cycling the  
catalysts between  $0.6$  and  $1.0 \text{ V (vs. RHE)}$  at  $50 \text{ mV s}^{-1}$  under  $\text{N}_2$  atmosphere in  
 $0.1 \text{ M KOH}$  and  $0.5 \text{ M H}_2\text{SO}_4$ .<sup>27, 31</sup>

**Fuel cell assembly.** The electrodes were prepared by spray-coating the  
catalyst ink on A201 alkaline membrane (Tokoyama, anion exchange capacity:  
 $1.7 \text{ mmol g}^{-1}$ , thickness:  $28 \text{ }\mu\text{m}$ ) at  $40^\circ\text{C}$ . The catalyst ink was prepared by  
ultrasonically dispersing the desired amount of catalyst in 2-propanol solution (Sigma-  
Aldrich) and AS-4 ionomer (Tokuyama,  $5 \text{ wt } \%$  solution, anion exchange  
capacity:  $1.5 \text{ mmol g}^{-1}$ ) for 30 minutes. The amount of AS-4 ionomer was kept  
at  $20 \text{ wt } \%$  for Fe-N-CC catalyst and  $15 \text{ wt } \%$  for commercial Pt/C (Sigma

1  
2  
3 Aldrich, 20 wt % Pt on graphitized carbon). The catalyst loading was calculated  
4  
5 by weighing the membrane before and after spray-coating, and kept at 0.2 mg  
6  
7  $\text{cm}^{-2}$  (total catalyst). Commercial Pt/C (Alfa Aesar, Pt 40 wt %) catalyst was  
8  
9 used as the anode catalyst with the loading fixed at 0.4  $\text{mg}_{\text{Pt}} \text{cm}^{-2}$ . The effective  
10  
11 electrode area was 5.29  $\text{cm}^2$ . The catalyst coated membrane (CCM) was  
12  
13 soaked in 0.1 M KOH overnight before testing.  
14  
15

16  
17 Each CCM was tested by fitting it between two gas diffusion layers and  
18  
19 mounted in single-cell hardware with a built-in reference electrode (Fuel Cell  
20  
21 Technologies Inc.). Fuel cell measurements were carried out using Scribner  
22  
23 890e test station (Scribner Associates). Electrochemical impedance  
24  
25 spectroscopy (EIS) measurements were carried out using Gamry Reference  
26  
27 3000AE (Gamry Instruments) in a three-electrode configuration to monitor both  
28  
29 the anode and cathode individually. The cell temperature was set at 50°C, and  
30  
31 the anode and cathode were fed with humidified (95% relative humidity)  $\text{H}_2$  and  
32  
33  $\text{O}_2$  at 0.5  $\text{L min}^{-1}$  and 1  $\text{L min}^{-1}$ , respectively. Prior to measurements, the CCM  
34  
35 was activated by maintaining the cell voltage at ~0.3 V for 1 hour. The EIS was  
36  
37 done at 10, 25, 50, and 100  $\text{mA cm}^{-2}$  in a frequency range of 0.1 – 10 kHz with  
38  
39 applied AC amplitude of 10% of the actual current.  
40  
41  
42  
43

#### 44 **Acknowledgments**

45  
46  
47 This research work was supported by the Spanish Ministerio de Economía y  
48  
49 Competitividad, MINECO (MAT2012-31651), Fondo Europeo de Desarrollo  
50  
51 Regional (FEDER) and FICYT Regional Project (GRUPIN14-102). G. A. F.  
52  
53 thanks the MINECO for his predoctoral contract and M. S. thanks the Spanish  
54  
55 Ministerio de Ciencia e Innovación for her Ramón y Cajal contract.  
56  
57  
58  
59  
60

1  
2  
3 **Supporting Information Available:** Comparative tables of N-doped and Fe-N-  
4 doped carbon materials in basic and acid media. Nitrogen sorption isotherm,  
5 XRD pattern, Raman spectra of and graphitic carbon regions, TGA analysis in  
6 air. XPS general spectrum and high-resolution Fe 2p<sub>3/2</sub> XPS spectrum. TEM  
7 image and its corresponding EDX mappings for C, N, O and Fe. HRTEM  
8 images of Fe<sub>3</sub>C nanoparticle. Cyclic voltammograms in N<sub>2</sub> and O<sub>2</sub> saturated 0.1  
9 M KOH and 0.5 M H<sub>2</sub>SO<sub>4</sub> electrolytes, LSV at 10 mV s<sup>-1</sup> in the presence of  
10 oxygen with rotation speed from 400 to 2400 rpm in 0.1 M KOH and 0.5 M  
11 H<sub>2</sub>SO<sub>4</sub>, Koutecky-Levich plots in 0.1 M KOH and 0.1 M H<sub>2</sub>SO<sub>4</sub>, comparison of  
12 the chronoamperometric response of Fe-N-CC and Pt/C over 10,000 s at 0.68 V  
13 and a constant rotation speed of 800 rpm in O<sub>2</sub>-saturated solution 0.1 M KOH,  
14 and Nyquist plots of the whole cell, including the half-cell measurements of the  
15 cathode This material is available free of charge *via* the Internet at  
16 <http://pubs.acs.org>.  
17  
18  
19  
20  
21  
22  
23  
24  
25  
26  
27  
28  
29  
30  
31  
32  
33  
34  
35  
36  
37  
38  
39  
40  
41  
42  
43  
44  
45  
46  
47  
48  
49  
50  
51  
52  
53  
54  
55  
56  
57  
58  
59  
60



## List of Tables and Figures

**Table 1.** Physico-chemical properties of the N-doped carbon capsules.

Sample code	$S_{\text{BET}}$ ( $\text{m}^2 \text{g}^{-1}$ )	$V_p$ ( $\text{cm}^3 \text{g}^{-1}$ ) <sup>a</sup>	Pore size (nm) <sup>b</sup>	$\alpha_s$ -plot results		C (wt %)	N (wt %)	O (wt %)	$\sigma$ ( $\text{S m}^{-1}$ )
				$V_m$ ( $\text{cm}^3 \text{g}^{-1}$ ) <sup>c</sup>	$S_{\text{ext}}$ ( $\text{m}^2 \text{g}^{-1}$ ) <sup>d</sup>				
Fe-N-CC	1590	1.46	3.8	1.28	92	83.28	5.88	10.04	22

<sup>a</sup> Pore volume determined at  $p/p_0=0.90$ . <sup>b</sup> Maximum of the KJS pore size distribution. <sup>c</sup> Volume of framework-confined mesopores. <sup>d</sup> External surface area.

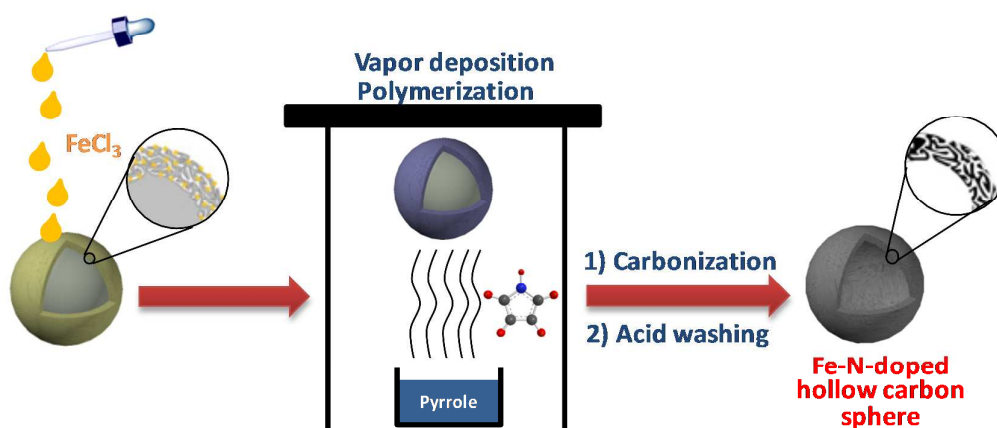


**Figure 1.** Schematic illustration of the synthesis procedure.

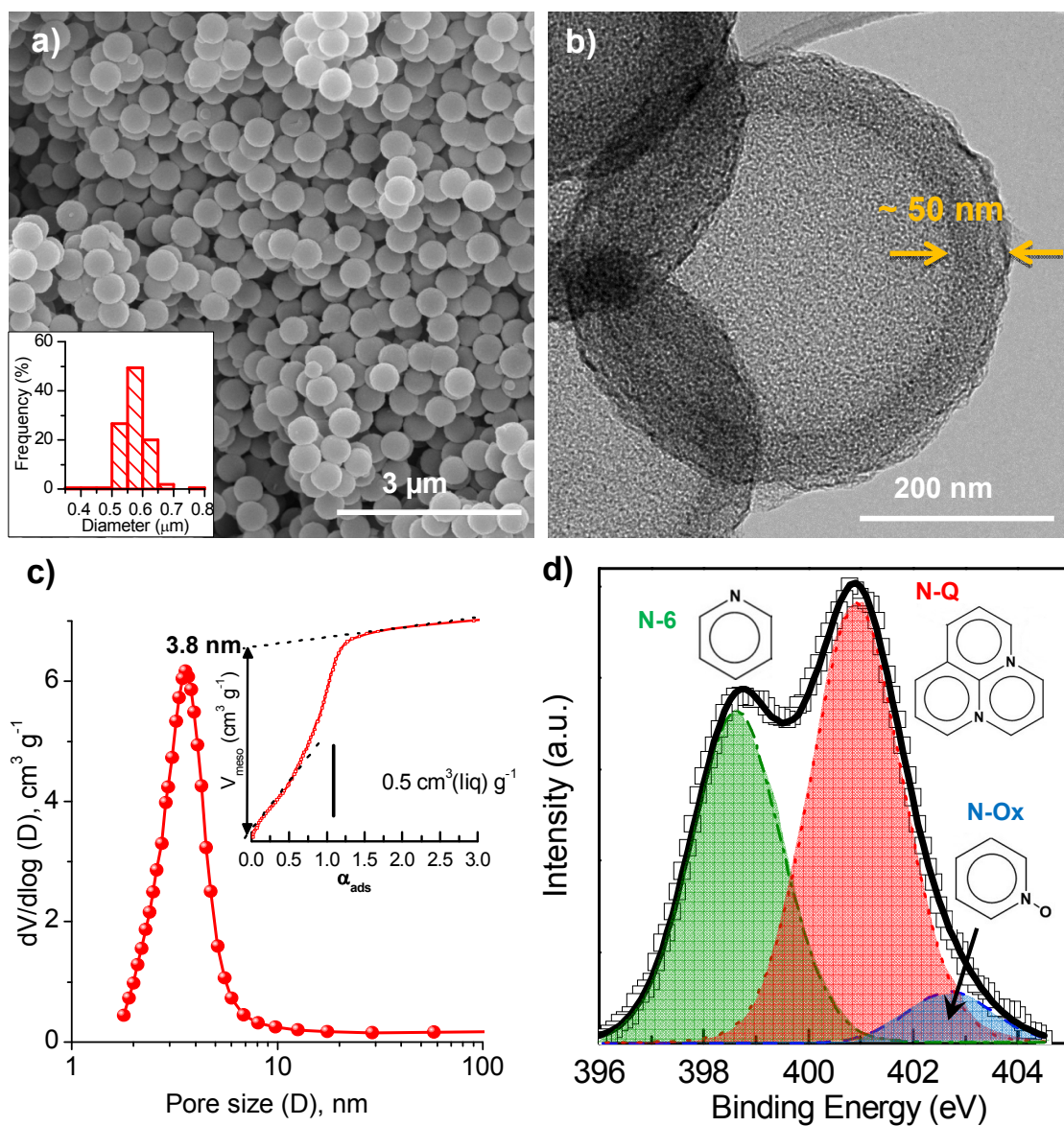


**Figure 2.** (a) SEM image of the hollow carbon capsules (inset: particle diameter distribution determined over 200 particles), (b) high-magnification TEM images of the hollow carbon capsules, (c) KJS pore size distribution and  $\alpha_s$ -plot method applied to the  $N_2$  adsorption branch (inset) and (d) XPS N 1s core level spectra of the Fe-N-doped carbon capsules (Fe-N-CC).

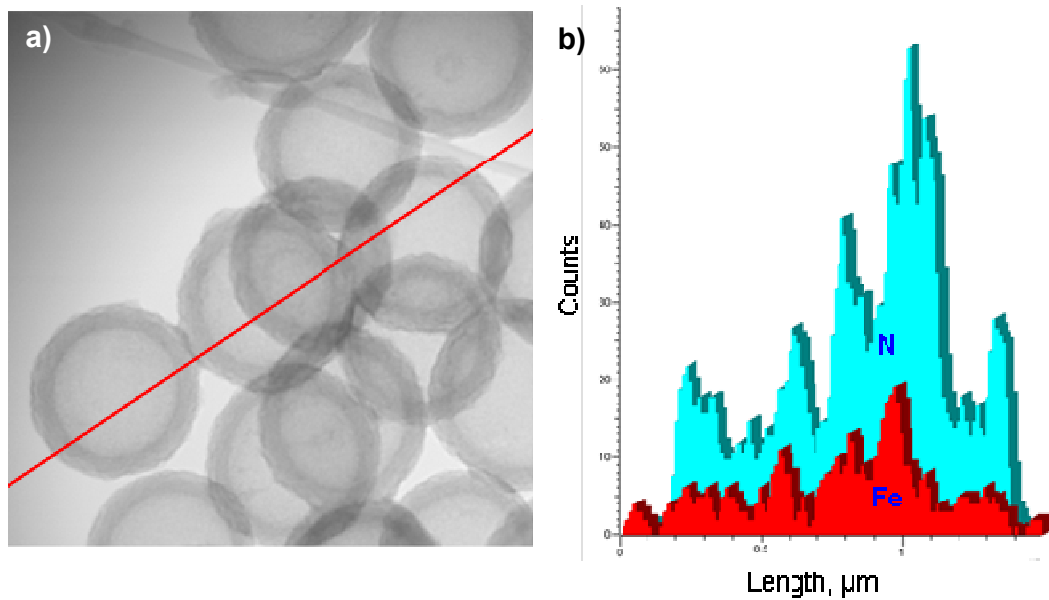


**Figure 3.** (a) TEM image of the Fe-N-CC carbon material and (b) its corresponding line profile concentration for nitrogen and iron.

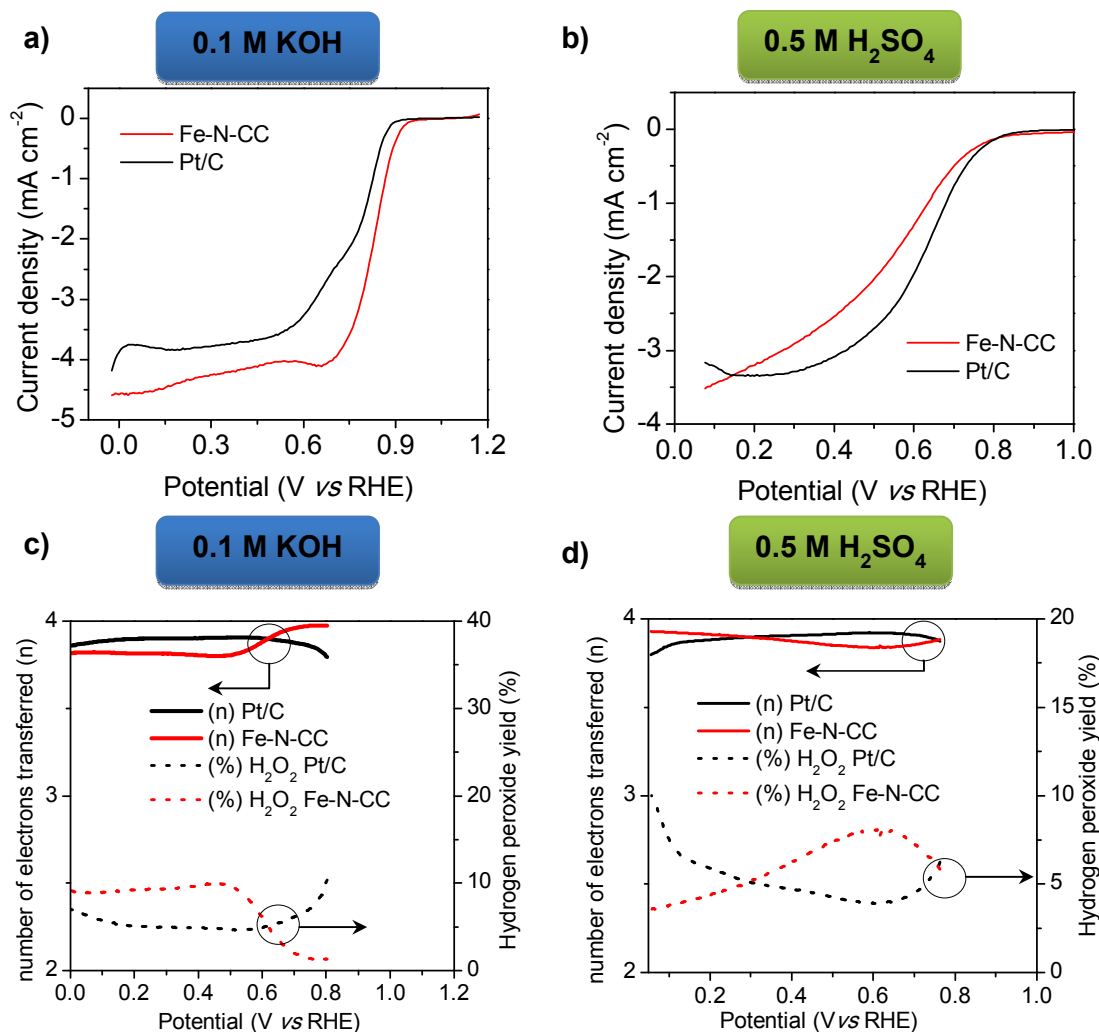


**Figure 4.** Comparison of the RDE polarization curves at 1600 rpm for Fe-N-CC and Pt/C catalysts in (a) 0.1 M KOH and (b) 0.1 M H<sub>2</sub>SO<sub>4</sub>, and number of electrons transferred and peroxide yield of the Fe-N-CC carbon capsules and Pt/C catalysis in (c) 0.1 M KOH and (d) 0.5 M H<sub>2</sub>SO<sub>4</sub>. The catalyst loadings were 0.1 mg cm<sup>-2</sup> for both Fe-N-CC and Pt/C catalysts.

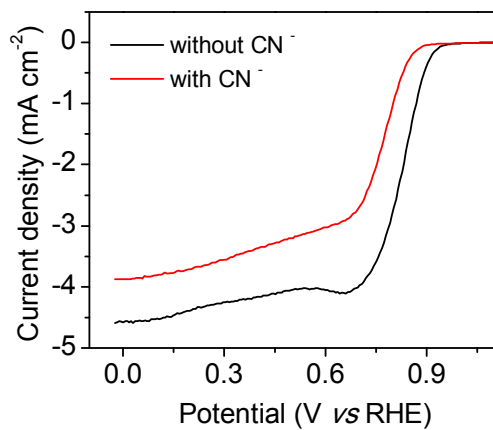


**Figure 5.** LSVs at  $10 \text{ mV s}^{-1}$  in the presence of oxygen at 1600 rpm in 0.1 M KOH without and in presence of cyanide ions (10 mM KCN).

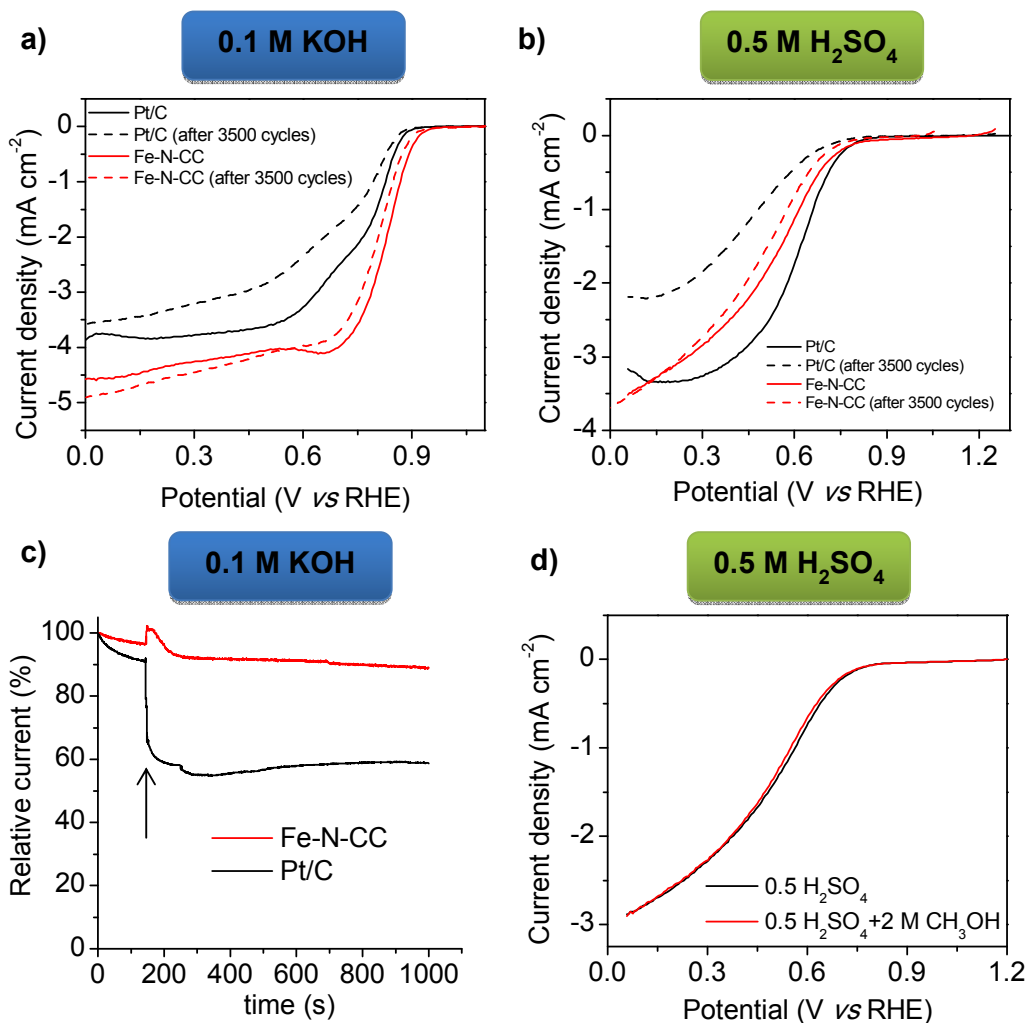


**Figure 6.** LSVs for Fe-N-CC and Pt/C at 1600 rpm in O<sub>2</sub>-saturated (a) 0.1 M KOH and (b) 0.5 M H<sub>2</sub>SO<sub>4</sub> before and after 3500 potential cycles, (c) comparison of the chronoamperometric response over 1000 s at a constant rotation speed of 1600 rpm in O<sub>2</sub>-saturated solution at 0.68 V for Fe-N-CC and Pt/C catalysts in 0.1 M KOH (the arrow indicates the addition of methanol) and (d) polarization curves of Fe-N-CC in O<sub>2</sub>-saturated 0.5 M H<sub>2</sub>SO<sub>4</sub> with (black) and without (red) 2 M methanol.

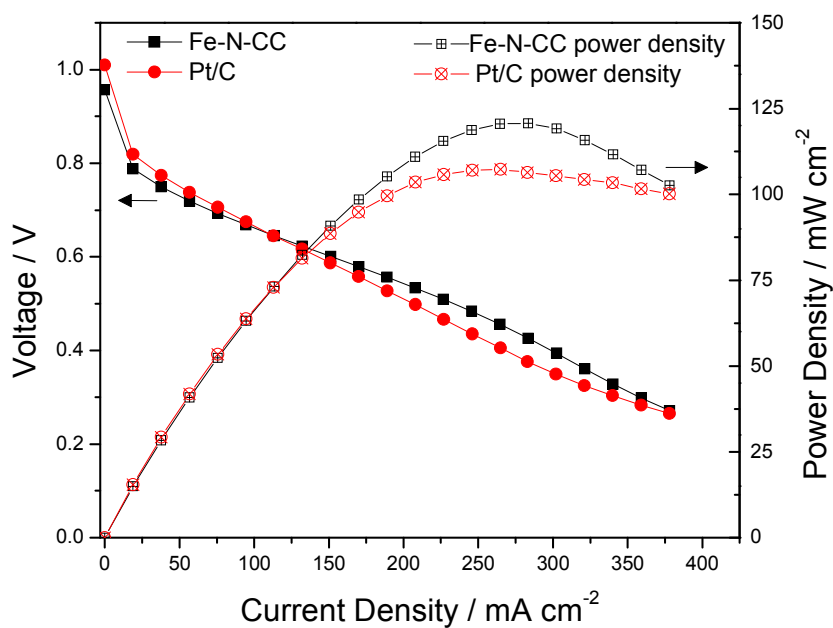


**Figure 7.** Polarization curve and power density of alkaline exchange membrane fuel cells operating at 50°C with Fe-N-CC and Pt/C as cathode catalysts (0.2 mg cm<sup>-2</sup>).

## References

1. Marković, N. M.; Schmidt, T. J.; Stamenković, V.; Ross, P. N. Oxygen Reduction Reaction on Pt and Pt Bimetallic Surfaces: A Selective Review. *Fuel Cells* **2001**, 1, 105-116.
2. Chen, Z.; Higgins, D.; Yu, A.; Zhang, L.; Zhang, J. A Review on Non-Precious Metal Electrocatalysts for PEM Fuel Cells. *Energy Environ. Sci.* **2011**, 4, 3167-3192.
3. Yu, D.; Nagelli, E.; Du, F.; Dai, L. Metal-Free Carbon Nanomaterials Become More Active than Metal Catalysts and Last Longer. *J. Phys. Chem. Lett.* **2010**, 1, 2165-2173.
4. Zhu, J.; Yang, D.; Yin, Z.; Yan, Q.; Zhang, H. Graphene and Graphene-Based Materials for Energy Storage Applications. *Small* **2014**, 10, 3480-3498.
5. Othman, R.; Dicks, A. L.; Zhu, Z. Non Precious Metal Catalysts for the PEM Fuel Cell Cathode. *Int. J. Hydrogen Energy* **2012**, 37, 357-372.
6. Jaouen, F.; Proietti, E.; Lefevre, M.; Chenitz, R.; Dodelet, J.-P.; Wu, G.; Chung, H. T.; Johnston, C. M.; Zelenay, P. Recent Advances in Non-Precious Metal Catalysis for Oxygen-Reduction Reaction in Polymer Electrolyte Fuel Cells. *Energy Environ. Sci.* **2011**, 4, 114-130.
7. Gorlin, Y.; Chung, C.-J.; Nordlund, D.; Clemens, B. M.; Jaramillo, T. F. Mn<sub>3</sub>O<sub>4</sub> Supported on Glassy Carbon: An Active Non-Precious Metal Catalyst for the Oxygen Reduction Reaction. *ACS Catal.* **2012**, 2, 2687-2694.
8. Hu, Y.; Jensen, J. O.; Zhang, W.; Cleemann, L. N.; Xing, W.; Bjerrum, N. J.; Li, Q. Hollow Spheres of Iron Carbide Nanoparticles Encased in Graphitic Layers as Oxygen Reduction Catalysts. *Angew. Chem. Int. Ed.* **2014**, 53, 3675-3679.
9. Dai, L.; Xue, Y.; Qu, L.; Choi, H.-J.; Baek, J.-B. Metal-Free Catalysts for Oxygen Reduction Reaction. *Chem. Rev.* **2015**, 115, 4823-4892.
10. Gong, K.; Du, F.; Xia, Z.; Durstock, M.; Dai, L. Nitrogen-Doped Carbon Nanotube Arrays with High Electrocatalytic Activity for Oxygen Reduction. *Science* **2009**, 323, 760-764.
11. Masa, J.; Xia, W.; Muhler, M.; Schuhmann, W. On the Role of Metals in Nitrogen-Doped Carbon Electrocatalysts for Oxygen Reduction. *Angew. Chem. Int. Ed.* **2015**, 54, 10102-10120.
12. Wang, D.-W.; Su, D. Heterogeneous Nanocarbon Materials for Oxygen Reduction Reaction. *Energy Environ. Sci.* **2014**, 7, 576-591.
13. Daems, N.; Sheng, X.; Vankelecom, I. F. J.; Pescarmona, P. P. Metal-Free Doped Carbon Materials as Electrocatalysts for the Oxygen Reduction reaction. *J. Mater. Chem. A* **2014**, 2, 4085-4110.
14. Shao, Y.; Sui, J.; Yin, G.; Gao, Y. Nitrogen-doped Carbon Nanostructures and Their Composites as Catalytic Materials for Proton Exchange Membrane Fuel Cell. *Appl. Catal. B* **2008**, 79, 89-99.
15. Qu, L.; Liu, Y.; Baek, J.-B.; Dai, L. Nitrogen-Doped Graphene as Efficient Metal-Free Electrocatalyst for Oxygen Reduction in Fuel Cells. *ACS Nano* **2010**, 4, 1321-1326.
16. Wu, K.-H.; Wang, D.-W.; Su, D.-S.; Gentle, I. R. A Discussion on the Activity Origin in Metal-Free Nitrogen-Doped Carbons For Oxygen Reduction Reaction and Their Mechanisms. *ChemSusChem* **2015**, 8, 2772-2788.
17. Yu, X.; Ye, S. Recent Advances in Activity and Durability Enhancement of Pt/C Catalytic Cathode in PEMFC: Part II: Degradation Mechanism and



1  
2  
3 Durability Enhancement of Carbon Supported Platinum Catalyst. *J. Power*  
4 *Sources* **2007**, 172, 145-154.

5 18. Yin, J.; Qiu, Y.; Yu, J. Enhanced Electrochemical Activity for Oxygen  
6 Reduction Reaction from Nitrogen-Doped Carbon Nanofibers by Iron Doping.  
7 *ECS Solid State Let.* **2013**, 2, M37-M39.

8 19. Mo, Z.; Liao, S.; Zheng, Y.; Fu, Z. Preparation of Nitrogen-Doped Carbon  
9 Nanotube Arrays and Their Catalysis Towards Cathodic Oxygen Reduction in  
10 Acidic and Alkaline Media. *Carbon* **2012**, 50, 2620-2627.

11 20. Vikkisk, M.; Kruusenberg, I.; Joost, U.; Shulga, E.; Tammeveski, K.  
12 Electrocatalysis of Oxygen Reduction on Nitrogen-Containing Multi-Walled  
13 Carbon Nanotube Modified Glassy Carbon Electrodes. *Electrochim. Acta* **2013**,  
14 87, 709-716.

15 21. Chen, Y.; Ma, R.; Zhou, Z.; Liu, G.; Zhou, Y.; Liu, Q.; Kaskel, S.; Wang,  
16 J. An *In Situ* Source-Template-Interface Reaction Route to 3D Nitrogen-Doped  
17 Hierarchical Porous Carbon as Oxygen Reduction Electrocatalyst. *Adv. Mater.*  
18 *Interfaces* **2015**, 2.

19 22. Liang, J.; Zheng, Y.; Chen, J.; Liu, J.; Hulicova-Jurcakova, D.; Jaroniec,  
20 M.; Qiao, S. Z. Facile Oxygen Reduction on a Three-Dimensionally Ordered  
21 Macroporous Graphitic C<sub>3</sub>N<sub>4</sub>/Carbon Composite Electrocatalyst. *Angew.*  
22 *Chem. Int. Ed.* **2012**, 51, 3892-3896.

23 23. Cong, H.-P.; Wang, P.; Gong, M.; Yu, S.-H. Facile Synthesis of  
24 Mesoporous Nitrogen-Doped Graphene: An Efficient Methanol-Tolerant  
25 Cathodic Catalyst for Oxygen Reduction Reaction. *Nano Energy* **2014**, 3, 55-63.

26 24. Chen, P.; Wang, L.-K.; Wang, G.; Gao, M.-R.; Ge, J.; Yuan, W.-J.; Shen,  
27 Y.-H.; Xie, A.-J.; Yu, S.-H. Nitrogen-Doped Nanoporous Carbon Nanosheets  
28 Derived From Plant Biomass: An Efficient Catalyst For Oxygen Reduction  
29 Reaction. *Energy Environ. Sci.* **2014**, 7, 4095-4103.

30 25. Zhou, M.; Yang, C.; Chan, K.-Y. Structuring Porous Iron-Nitrogen-Doped  
31 Carbon in a Core/Shell Geometry for the Oxygen Reduction Reaction. *Adv.*  
32 *Energy Mater.* **2014**, 4.

33 26. Zhong, H.; Deng, C.; Qiu, Y.; Yao, L.; Zhang, H. Nitrogen-Doped  
34 Hierarchically Porous Carbon as Efficient Oxygen Reduction Electrocatalysts in  
35 Acid Electrolyte. *J. Mater. Chem. A* **2014**, 2, 17047-17057.

36 27. Li, Y.; Zhou, W.; Wang, H.; Xie, L.; Liang, Y.; Wei, F.; Idrobo, J.-C.;  
37 Pennycook, S. J.; Dai, H. An Oxygen Reduction Electrocatalyst Based on  
38 Carbon Nanotube-Graphene Complexes. *Nat. Nano* **2012**, 7, 394-400.

39 28. Zhang, J.; Zhao, Z.; Xia, Z.; Dai, L. A Metal-Free Bifunctional  
40 Electrocatalyst for Oxygen Reduction and Oxygen Evolution Reactions. *Nat.*  
41 *Nano* **2015**, 10, 444-452.

42 29. Yu, D.; Zhang, Q.; Dai, L. Highly Efficient Metal-Free Growth of Nitrogen-  
43 Doped Single-Walled Carbon Nanotubes on Plasma-Etched Substrates for  
44 Oxygen Reduction. *J. Am. Chem. Soc.* **2010**, 132, 15127-15129.

45 30. Parvez, K.; Yang, S.; Hernandez, Y.; Winter, A.; Turchanin, A.; Feng, X.;  
46 Müllen, K. Nitrogen-Doped Graphene and Its Iron-Based Composite As Efficient  
47 Electrocatalysts for Oxygen Reduction Reaction. *ACS Nano* **2012**, 6, 9541-  
48 9550.

49 31. Wu, G.; More, K. L.; Johnston, C. M.; Zelenay, P. High-Performance  
50 Electrocatalysts for Oxygen Reduction Derived from Polyaniline, Iron, and  
51 Cobalt. *Science* **2011**, 332, 443-447.

- 1  
2  
3 32. Masa, J.; Zhao, A.; Xia, W.; Sun, Z.; Mei, B.; Muhler, M.; Schuhmann, W.  
4 Trace Metal Residues Promote the Activity of Supposedly Metal-Free Nitrogen-  
5 Modified Carbon Catalysts for the Oxygen Reduction Reaction. *Electrochem.*  
6 *Commun.* **2013**, 34, 113-116.  
7  
8 33. Jin, X.; Zhang, G.; Hao, Y.; Chang, Z.; Sun, X. Residual Metals Present  
9 in "Metal-Free" N-Doped Carbons. *Chem. Commun.* **2015**, 51, 15585-15587.  
10  
11 34. Ranjbar Sahraie, N.; Paraknowitsch, J. P.; Göbel, C.; Thomas, A.;  
12 Strasser, P. Noble-Metal-Free Electrocatalysts with Enhanced ORR  
13 Performance by Task-Specific Functionalization of Carbon using Ionic Liquid  
14 Precursor Systems. *J. Am. Chem. Soc.* **2014**, 136, 14486-14497.  
15  
16 35. Lin, L.; Zhu, Q.; Xu, A.-W. Noble-Metal-Free Fe-N/C Catalyst for Highly  
17 Efficient Oxygen Reduction Reaction under Both Alkaline and Acidic Conditions.  
18 *J. Am. Chem. Soc.* **2014**, 136, 11027-11033.  
19  
20 36. Sevilla, M.; Yu, L.; Fellingner, T. P.; Fuertes, A. B.; Titirici, M.-M.  
21 Polypyrrole-Derived Mesoporous Nitrogen-Doped Carbons with Intrinsic  
22 Catalytic Activity in the Oxygen Reduction Reaction. *RSC Adv.* **2013**, 3, 9904-  
23 9910.  
24  
25 37. Chao, S.; Lu, Z.; Bai, Z.; Cui, Q.; Qiao, J.; Yang, Z.; Yang, L. Tuning  
26 Synthesis of Highly Active Nitrogen-Doped Graphite and Determining the  
27 Optimal Structure from First-Principles Calculations. *Int. J. Electrochem. Sci.*  
28 **2013**, 8, 8786-8799.  
29  
30 38. Wu, Z.-Y.; Xu, X.-X.; Hu, B.-C.; Liang, H.-W.; Lin, Y.; Chen, L.-F.; Yu, S.-  
31 H. Iron Carbide Nanoparticles Encapsulated in Mesoporous Fe-N-Doped  
32 Carbon Nanofibers for Efficient Electrocatalysis. *Angew. Chem. Int. Ed.* **2015**,  
33 54, 8179-8183.  
34  
35 39. Sevilla, M.; Fuertes, A. B. Catalytic Graphitization of Templated  
36 Mesoporous Carbons. *Carbon* **2006**, 44, 468-474.  
37  
38 40. Sevilla, M.; Sanchis, C.; Valdes-Solis, T.; Morallon, E.; Fuertes, A. B.  
39 Synthesis of Graphitic Carbon Nanostructures from Sawdust and Their  
40 Application as Electrocatalyst Supports. *J. Phys. Chem. C* **2007**, 111, 9749-  
41 9756.  
42  
43 41. Ōya, A.; Marsh, H. Phenomena of Catalytic Graphitization. *J. Mater. Sci.*  
44 **1982**, 17, 309-322.  
45  
46 42. Pels, J. R.; Kapteijn, F.; Moulijn, J. A.; Zhu, Q.; Thomas, K. M. Evolution  
47 of Nitrogen Functionalities in Carbonaceous Materials During Pyrolysis. *Carbon*  
48 **1995**, 33, 1641-1653.  
49  
50 43. Schmiers, H.; Friebel, J.; Streubel, P.; Hesse, R.; Köpsel, R. Change of  
51 Chemical Bonding of Nitrogen of Polymeric N-Heterocyclic Compounds During  
52 Pyrolysis. *Carbon* **1999**, 37, 1965-1978.  
53  
54 44. Tylus, U.; Jia, Q.; Strickland, K.; Ramaswamy, N.; Serov, A.; Atanassov,  
55 P.; Mukerjee, S. Elucidating Oxygen Reduction Active Sites in Pyrolyzed Metal-  
56 Nitrogen Coordinated Non-Precious-Metal Electrocatalyst Systems. *J. Phys.*  
57 *Chem. C* **2014**, 118, 8999-9008.  
58  
59 45. Wei, J.; Liang, Y.; Hu, Y.; Kong, B.; Simon, G. P.; Zhang, J.; Jiang, S. P.;  
60 Wang, H. A Versatile Iron-Tannin-Framework Ink Coating Strategy to Fabricate  
Biomass-Derived Iron Carbide/Fe-N-Carbon Catalysts for Efficient Oxygen  
Reduction. *Angew. Chem. Int. Ed.* **2016**, 55, 1355-1359.  
46. Ferrero, G. A.; Fuertes, A. B.; Sevilla, M. N-Doped Porous Carbon  
Capsules with Tunable Porosity for High-Performance Supercapacitors. *J.*  
*Mater. Chem. A* **2015**, 3, 2914-2923.

- 1  
2  
3 47. Liu, R.; Wu, D.; Feng, X.; Müllen, K. Nitrogen-Doped Ordered  
4 Mesoporous Graphitic Arrays with High Electrocatalytic Activity for Oxygen  
5 Reduction. *Angew. Chem. Int. Ed.* **2010**, *49*, 2565-2569.
- 6 48. He, W.; Jiang, C.; Wang, J.; Lu, L. High-Rate Oxygen Electroreduction  
7 over Graphitic-N Species Exposed on 3D Hierarchically Porous Nitrogen-Doped  
8 Carbons. *Angew. Chem. Int. Ed.* **2014**, *53*, 9503-9507.
- 9 49. Wei, W.; Liang, H.; Parvez, K.; Zhuang, X.; Feng, X.; Müllen, K. Nitrogen-  
10 Doped Carbon Nanosheets with Size-Defined Mesopores as Highly Efficient  
11 Metal-Free Catalyst for the Oxygen Reduction Reaction. *Angew. Chem.* **2014**,  
12 *126*, 1596-1600.
- 13 50. You, C.; Liao, S.; Qiao, X.; Zeng, X.; Liu, F.; Zheng, R.; Song, H.; Zeng,  
14 J.; Li, Y. Conversion of Polystyrene Foam to a High-Performance Doped  
15 Carbon Catalyst with Ultrahigh Surface Area and Hierarchical Porous Structures  
16 for Oxygen Reduction. *J. Mater. Chem. A* **2014**, *2*, 12240-12246.
- 17 51. Liu, J.; Sun, X.; Song, P.; Zhang, Y.; Xing, W.; Xu, W. High-Performance  
18 Oxygen Reduction Electrocatalysts based on Cheap Carbon Black, Nitrogen,  
19 and Trace Iron. *Adv. Mater.* **2013**, *25*, 6879-6883.
- 20 52. Zhang, C.; Antonietti, M.; Fellingner, T.-P. Blood Ties: Co<sub>3</sub>O<sub>4</sub> Decorated  
21 Blood Derived Carbon as a Superior Bifunctional Electrocatalyst. *Adv. Funct.*  
22 *Mater.* **2014**, *24*, 7655-7665.
- 23 53. Wu, Z.; Li, W.; Xia, Y.; Webley, P.; Zhao, D. Ordered Mesoporous  
24 Graphitized Pyrolytic Carbon Materials: Synthesis, Graphitization, and  
25 Electrochemical Properties. *J. Mater. Chem.* **2012**, *22*, 8835-8845.
- 26 54. Tang, J.; Liu, J.; Li, C.; Li, Y.; Tade, M. O.; Dai, S.; Yamauchi, Y.  
27 Synthesis of Nitrogen-Doped Mesoporous Carbon Spheres with Extra-Large  
28 Pores through Assembly of Diblock Copolymer Micelles. *Angew. Chem. Int. Ed.*  
29 **2015**, *54*, 588-593.
- 30 55. Xiao, H.; Shao, Z.-G.; Zhang, G.; Gao, Y.; Lu, W.; Yi, B. Fe-N-carbon  
31 Black for the Oxygen Reduction Reaction in Sulfuric Acid. *Carbon* **2013**, *57*,  
32 443-451.
- 33 56. Liu, X.; Zhu, H.; Yang, X. One-Step Synthesis of Dopamine-Derived  
34 Micro/Mesoporous Nitrogen-Doped Carbon Materials for Highly Efficient  
35 Oxygen-Reduction Catalysts. *J. Power Sources* **2014**, *262*, 414-420.
- 36 57. Yang, T.; Liu, J.; Zhou, R.; Chen, Z.; Xu, H.; Qiao, S. Z.; Monteiro, M. J.  
37 N-Doped Mesoporous Carbon Spheres as the Oxygen Reduction Reaction  
38 Catalysts. *J. Mater. Chem. A* **2014**, *2*, 18139-18146.
- 39 58. Li, J.; Li, Z.; Tong, J.; Xia, C.; Li, F. Nitrogen-Doped Ordered Mesoporous  
40 Carbon Sphere with Short Channel as an Efficient Metal-Free Catalyst for  
41 Oxygen Reduction Reaction. *RSC Adv.* **2015**, *5*, 70010-70016.
- 42 59. Hu, C.; Wang, L.; Zhao, Y.; Ye, M.; Chen, Q.; Feng, Z.; Qu, L. Designing  
43 Nitrogen-Enriched Echinus-Like Carbon Capsules for Highly Efficient Oxygen  
44 Reduction Reaction and Lithium Ion Storage. *Nanoscale* **2014**, *6*, 8002-8009.
- 45 60. Shih, Y.-H.; Sagar, G. V.; Lin, S. D. Effect of Electrode Pt Loading on the  
46 Oxygen Reduction Reaction Evaluated by Rotating Disk Electrode and Its  
47 Implication on the Reaction Kinetics. *J. Phys. Chem. C* **2008**, *112*, 123-130.
- 48 61. Alonso-Vante, N. Platinum and Non-Platinum Nanomaterials for the  
49 Molecular Oxygen Reduction Reaction. *ChemPhysChem* **2010**, *11*, 2732-2744.
- 50 62. Zhang, J. PEM Fuel Cell Electrocatalysts and Catalyst Layers:  
51 Fundamentals and Applications. Springer Science & Business Media: 2008.
- 52  
53  
54  
55  
56  
57  
58  
59  
60

- 1  
2  
3 63. Thorum, M. S.; Hankett, J. M.; Gewirth, A. A. Poisoning the Oxygen  
4 Reduction Reaction on Carbon-Supported Fe and Cu Electrocatalysts:  
5 Evidence for Metal-Centered Activity. *J. Phys. Chem. Lett.* **2011**, *2*, 295-298.
- 6 64. Liang, Y.; Li, Y.; Wang, H.; Zhou, J.; Wang, J.; Regier, T.; Dai, H. Co<sub>3</sub>O<sub>4</sub>  
7 Nanocrystals on Graphene as a Synergistic Catalyst for Oxygen Reduction  
8 Reaction. *Nat. Mater* **2011**, *10*, 780-786.
- 9 65. Liang, H.-W.; Zhuang, X.; Brüller, S.; Feng, X.; Müllen, K. Hierarchically  
10 Porous Carbons with Optimized Nitrogen Doping as Highly Active  
11 Electrocatalysts for Oxygen Reduction. *Nat. Commun* **2014**, *5*.
- 12 66. Ai, K.; Liu, Y.; Ruan, C.; Lu, L.; Lu, G. Sp<sup>2</sup> C-Dominant N-Doped Carbon  
13 Sub-micrometer Spheres with a Tunable Size: A Versatile Platform for Highly  
14 Efficient Oxygen-Reduction Catalysts. *Adv. Mater.* **2013**, *25*, 998-1003.
- 15 67. Zhang, L.; Su, Z.; Jiang, F.; Yang, L.; Qian, J.; Zhou, Y.; Li, W.; Hong, M.  
16 Highly Graphitized Nitrogen-Doped Porous Carbon Nanopolyhedra Derived  
17 from ZIF-8 Nanocrystals as Efficient Electrocatalysts for Oxygen Reduction  
18 Reactions. *Nanoscale* **2014**, *6*, 6590-6602.
- 19 68. Qiu, K.; Guo, Z. X. Hierarchically Porous Graphene Sheets and Graphitic  
20 Carbon Nitride Intercalated Composites for Enhanced Oxygen Reduction  
21 Reaction. *J. Mater. Chem. A* **2014**, *2*, 3209-3215.
- 22 69. Geng, D.; Chen, Y.; Chen, Y.; Li, Y.; Li, R.; Sun, X.; Ye, S.; Knights, S.  
23 High Oxygen-Reduction Activity and Durability of Nitrogen-Doped Graphene.  
24 *Energy Environ. Sci.* **2011**, *4*, 760-764.
- 25 70. Chai, G. S.; Shin, I.; Yu, J. S. Synthesis of Ordered, Uniform,  
26 Macroporous Carbons with Mesoporous Walls Templated by Aggregates of  
27 Polystyrene Spheres and Silica Particles for Use as Catalyst Supports in Direct  
28 Methanol Fuel Cells. *Adv. Mater.* **2004**, *16*, 2057-2061.
- 29 71. Neburchilov, V.; Martin, J.; Wang, H.; Zhang, J. A review of Polymer  
30 Electrolyte Membranes for Direct Methanol Fuel Cells. *J. Power Sources* **2007**,  
31 *169*, 221-238.
- 32 72. Du, C. Y.; Zhao, T. S.; Xu, C. Simultaneous Oxygen-Reduction and  
33 Methanol-Oxidation Reactions at the Cathode of a DMFC: A model-Based  
34 Electrochemical Impedance Spectroscopy Study. *J. Power Sources* **2007**, *167*,  
35 265-271.
- 36 73. Larminie, J.; Dicks, A.; McDonald, M. S. Fuel Cell Systems Explained.  
37 Wiley New York: 2003; Vol. 2.
- 38 74. Büchel, G.; Unger, K. K.; Matsumoto, A.; Tsutsumi, K. A Novel Pathway  
39 for Synthesis of Submicrometer-Size Solid Core/Mesoporous Shell Silica  
40 Spheres. *Adv. Mater.* **1998**, *10*, 1036-1038.
- 41 75. Kruk, M.; Jaroniec, M.; Sayari, A. Application of Large Pore MCM-41  
42 Molecular Sieves To Improve Pore Size Analysis Using Nitrogen Adsorption  
43 Measurements. *Langmuir* **1997**, *13*, 6267-6273.
- 44 76. Kruk, M.; Jaroniec, M.; Gadkaree, K. P. Nitrogen Adsorption Studies of  
45 Novel Synthetic Active Carbons. *J. Colloid Interface Sci.* **1997**, *192*, 250-256.
- 46 77. Wu, Z.-Y.; Xu, X.-X.; Hu, B.-C.; Liang, H.-W.; Lin, Y.; Chen, L.-F.; Yu, S.-  
47 H. Iron Carbide Nanoparticles Encapsulated in Mesoporous Fe-N-Doped  
48 Carbon Nanofibers for Efficient Electrocatalysis. *Angew. Chem. Int. Ed.* **2015**,  
49 *54*, 8179-8183.
- 50 78. Lide, D. R. *CRC handbook of chemistry and physics*. CRC press: 2004.
- 51  
52  
53  
54  
55  
56  
57  
58  
59  
60

- 1  
2  
3 79. Gasteiger, H. A.; Ross, P. N. Oxygen Reduction on Platinum Low-Index  
4 Single-Crystal Surfaces in Alkaline Solution: Rotating Ring DiskPt(hkl) Studies.  
5 *J. Phys. Chem.* **1996**, 100, 6715-6721.  
6 80. Wu, J.; Jin, C.; Yang, Z.; Tian, J.; Yang, R. Synthesis of Phosphorus-  
7 Doped Carbon Hollow Spheres as Efficient Metal-Free Electrocatalysts for  
8 Oxygen Reduction. *Carbon* **2015**, 82, 562-571.  
9 81. Xing, W.; Yin, G.; Zhang, J. *Rotating Electrode Methods and Oxygen*  
10 *Reduction Electrocatalysts*. Elsevier: 2014.  
11  
12  
13  
14  
15  
16  
17  
18  
19  
20  
21  
22  
23  
24  
25  
26  
27  
28  
29  
30  
31  
32  
33  
34  
35  
36  
37  
38  
39  
40  
41  
42  
43  
44  
45  
46  
47  
48  
49  
50  
51  
52  
53  
54  
55  
56  
57  
58  
59  
60

## Table of Contents

Fe-N-doped mesoporous carbon capsules were employed as an electrocatalyst for the oxygen reduction reaction (ORR). The catalysts exhibited high catalytic activity and a remarkable stability in both acid and basic media.

